Photoreactions of Mercury in Surface Ocean Water: Gross Reaction Kinetics and Possible Pathways

ARTICLE *in* ENVIRONMENTAL SCIENCE AND TECHNOLOGY · DECEMBER 2009

Impact Factor: 5.33 · DOI: 10.1021/es9012728 · Source: PubMed

5 AUTHORS, INCLUDING:

N.J. O'Driscoll
Acadia University
65 PUBLICATIONS **880** CITATIONS
SEE PROFILE

Matthew MacLeod
Stockholm University
154 PUBLICATIONS **3,869** CITATIONS
SEE PROFILE

Bobby Neuhold
Eawag: Das Wasserforschungs-Institut des …
35 PUBLICATIONS **882** CITATIONS
SEE PROFILE

Environ. Sci. Technol. xxx, 000–000

Photoreactions of Mercury in Surface Ocean Water: Gross Reaction Kinetics and Possible Pathways

ASIF QURESHI,[†] NELSON O'DRISCOLL,[‡] MATTHEW MACLEOD,*[,†] YORCK-MICHAEL NEUHOLD,[†] AND KONRAD HUNGERBÜHLER[†]

Safety and Environmental Technology Group, ICB, ETH Zürich, Zürich 8093, Switzerland, and Earth and Environmental Sciences, Acadia University, Wolfville B4P 2R6, Canada

Received April 29, 2009. Revised manuscript received November 17, 2009. Accepted November 19, 2009.

We present pseudofirst order rate constants for gross photoreduction and gross photooxidation of mercury in surface water from the open Atlantic Ocean, determined under controlled laboratory conditions. Experiments using both unfiltered and filtered ocean water were carried out to characterize the relative importance of microbes and colloids on reaction kinetics. Results indicate that reduction and oxidation of mercury in ocean water does not follow a simple two-species reversible reaction pathway. We suggest two possible redox pathways that reproduce the pattern of dissolved gaseous mercury (DGM) concentrations observed in our laboratory experiments, and evaluate them using a controlled outdoor experiment. In both proposed pathways Hg(0), the major constituent of DGM, is converted to an unidentified oxidized species that is different from the reducible form present initially. This reaction step plays a major role in the net formation of DGM in our experiments. Our results represent new quantitative information about the gross reaction kinetics for both reduction and oxidation of mercury in open ocean surface water. Pseudofirst order rate constants for reduction reactions that form DGM were determined to be in the range of 0.15—0.93 h^{-1} and pseudofirst order rate constants for oxidation of Hg(0) to be in the range of 0.4—1.9 h^{-1}. Microbes and colloids did not appreciably influence the reduction and oxidation kinetics.

1. Introduction

Mercury is a pollutant of global concern known to travel large distances in the atmosphere into remote locations. It is estimated that oceans account for about one-third of total mercury flux to the atmosphere (*1*). The flux of mercury from the oceans is in the form of gaseous mercury which evades to the atmosphere. In the surface ocean, dissolved gaseous mercury (DGM), which is predominantly elemental mercury, Hg(0) (*2*), is produced as a net result of (i) reduction of divalent mercury species, Hg(II), and (ii) oxidation of Hg(0) to Hg(II). Thus, reduction and oxidation of mercury in surface oceans are important processes that influence the amount of DGM available for evasion, and play an important role in the global mercury cycle.

Reduction of Hg(II) to Hg(0) can be both photochemically mediated (*3*—*5*) and microbially mediated (*6, 7*). Oxidation of Hg(0) is also reported to be mediated both photochemically (*8*—*10*) and microbially (*7*). The net result of these reduction and oxidation reactions, in combination with water-to-air volatilization of mercury, is the well-documented diel (24 h) variation of DGM in natural waters (e.g.. refs *11 and 12)*. This diel variation is characterized by increasing DGM concentration in surface water after sunrise, with a maximum near the time of maximum solar radiation and a decrease thereafter. The diel variation thus indicates that net DGM formation is dependent on the intensity of incident radiation (e.g., ref *13*). Furthermore, ultraviolet (UV) radiation is likely the main driver for the two redox reactions (*2, 10, 14, 15*), although the effect of visible radiation cannot be entirely ruled out (*2*).

Not all Hg(II) compounds in natural waters are present in an easily reducible form (*16*). For example, in a mass balance analysis by O'Driscoll et al. (*15*), reducible mercury in freshwater lakes accounted only for about 40% of the total mercury. It has been hypothesized that Hg(II) must be complexed with dissolved organic matter (DOM) in order for Hg(II) photoreduction to take place (*17, 18*); reduction then takes place via electron transfer from the organic ligand to mercury (*17, 19*). This process has been shown to be inhibited in the presence of ligands such as chlorides that may compete with organic matter for binding with mercury (*17*).

Photooxidation of Hg(0) may be carried out by hydroxyl radicals that are produced, for example, by photolysis of nitrate/nitrite (*8*) or Fe(III)-organic acid coordination compounds (*4*). Photooxidation of Hg(0) by oxyhalide radicals (e.g., OCl^-, OBr^-) is also possible, but has not yet been reported in natural waters (*20*). Some "dark" oxidation in the absence of light (*2, 4*) is also carried out by hydroxyl radicals produced, via the Fenton reaction, from the photochemically produced hydrogen peroxide (*4*). Thus, some amount of light exposure prior to the dark period is required (*4, 9*) to have dark oxidation, with the kinetics of reaction depending on the intensity and duration of prior light exposure (*13, 21*).

In summary, many mechanisms have been proposed; however, which mechanisms may be relevant and dominant in natural systems is highly uncertain. In the absence of a complete mechanistic understanding of reduction and oxidation of mercury in surface waters, pseudofirst order rate constants determined experimentally under controlled conditions are useful to describe the system. For example, both reduction and oxidation of mercury have been modeled as pseudofirst order reactions (*15, 22, 23*). Further justifications for using pseudofirst order kinetics are discussed in Supporting Information (SI) Section S1.

To date, experimentally determined pseudofirst order rate constants for reduction and oxidation of mercury have been reported for freshwater (*13, 15*) and near-shore coastal, estuarine, and coastal shelf waters (e.g., refs *2, and 20)*, but they are not yet available for ocean water collected far from shore. The lack of information about reduction and oxidation reactions in the open ocean is evident in the most recent attempts to model mercury cycling between ocean and atmosphere (e.g., ref *16*) or over the whole globe (e.g., ref *24*). The models use empirically parametrized rate constants that were not determined from experiments, but rather that were selected so the observations can be reproduced. Moreover,

* Corresponding author phone: +41 44 632 3171; fax: +41 44 632 1189; e-mail: macleod@chem.ethz.ch.
[†] Safety and Environmental Technology Group.
[‡] Acadia University.

10.1021/es9012728

these studies parametrized a rate constant only for *net* reduction of Hg(II) to Hg(0), and did not differentiate between reduction and oxidation processes. Therefore, it is not possible to separate the influence of individual processes on the overall mercury profile. In addition, the values of these rate constants for ocean water are highly uncertain (*16*), and the pathways of reaction in the surface ocean are poorly understood. For these reasons, Pirrone et al. (*25*) recently highlighted the need to evaluate the formation of DGM in the surface microlayer of the oceans since it is an important gap in our understanding of the ocean-air component of the global mercury cycle.

The goal of the work reported here was to experimentally determine pseudofirst order rate constants for gross reduction and gross oxidation of mercury in water samples from the open ocean, in a controlled laboratory environment. Experiments were performed under two different intensities each of UV-A and UV-B radiation, to make an assessment of the contribution of the two wavelengths to redox reactions and to obtain first estimates of the dependence of the pseudofirst order rate constants on radiation intensity. Both filtered and unfiltered samples were analyzed to explore the contribution of microbes and colloids.

Since results from our experiments provided new information on the redox pathway for mercury in ocean water, the implied pathway was also evaluated against a controlled experiment monitoring the diel variation of DGM in ocean water.

2. Materials and Methods

2.1. Samples. Samples of ocean water were collected by the Bedford Institute of Oceanography from the open Atlantic Ocean (41°51′N, 60°46′W) at a depth of 3 m below the surface. Samples were stored in the dark in four high density polyethylene containers which had been washed with 20% hydrochloric acid (HCl) followed by double-deionized (d.i.) water (*15, 23*). This method minimizes mercury contamination and the introduction of chemicals that influence mercury reactions (*7*). The ocean water containers were kept under dark refrigeration at 4 °C until transportation to Acadia University, where they were frozen at −8 °C until the time of the experiments. Most microorganisms are expected to survive this freezing temperature (*26*). During the experiments, one container at a time was thawed and stored in the dark at 4 °C, and subsamples from this container were used. Ocean water in one container was consumed in approximately two weeks of experimental time.

2.2. Instrumentation. A LuzChem ICH-2 photo reactor was used for irradiating samples with UV-A or UV-B radiation. A maximum of eight UV lamps can be used in the photoreactor (Figure 1). The temperature inside the photoreactor was maintained at 25 ± 1 °C by means of an internal exhaust fan. For measurement of DGM, samples were purged with zero-Hg air and the DGM in the outgoing purge gas stream was measured using a Tekran 2537B analyzer. The Tekran 2537B analyzer can provide continuous measurements of DGM concentrations, with values logged every five minutes. The manufacturer reports its detection limit to be <0.1 ng/m^3, in a 7.5 L sample. Additional hardware required for the Tekran analyzer consisted of a zero-Hg air source (Tekran model 1100, see SI Section S2 for more information) and a data logging computer (Figure 1). Further details of the apparatus are described in O'Driscoll et al. (*15*).

All samples were analyzed in high quality fused silica quartz beakers (6 cm diameter, 9.6 cm height, from QSI scientific; approximately 270 mL in volume) with platinum cured silicone stoppers on the top. Before the start of any experiment, all beakers and stoppers were precleaned with 20% HCl and d.i. water, and irradiated simultaneously with UV-A and UV-B radiation until no detectable Hg(0) was liberated from the beaker or stopper walls. It should be noted that the relatively small radius of the beakers allows full transmission of radiation. Therefore, the rate constant values obtained in this work apply to the top few centimeters of surface ocean where there is full light penetration.

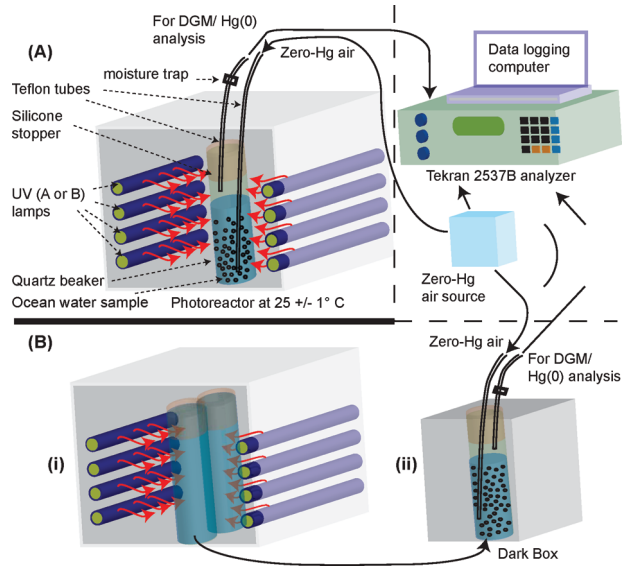

FIGURE 1. Experimental apparatus for (A) gross photoreduction experiment and (B) net photoreduction experiment.

2.3. Experimental Variables. Pseudofirst order rate constants for reduction and oxidation of mercury were determined for four radiation scenarios for both filtered and unfiltered ocean water.

2.3.1. Radiation Scenarios. Experiments were performed for two sets of radiation intensities each of UV-A and UV-B radiation (lamp spectra provided in SI Figure S1). For our experiments, the selected UV-A intensities were 15.24 W m^{-2} and 26.67 W m^{-2}. These corresponded to 39 and 68% of the full sun's intensity at Wolfville, Canada (45°05′N, 64° 22′W) on 25th July, 2008. Selected UV-B intensities were 2.35 W m^{-2} and 7.05 W m^{-2} which corresponded to 66 and 200% of full sun's intensity, respectively.

2.3.2. Filtered vs Unfiltered Samples. To examine the influence of microbes and colloids, samples were vacuum filtered through presterilized Omega polyethersulfone disk filters of pore size 0.2 μm (Pall Supor) using an all glass vacuum filtration flask and base. All microbes are expected to be removed by this filtration (*26*). Siciliano et al. (*7*) have noticed that samples filtered in the same manner remained sterile for up to 48 h. All glassware used for filtration was first autoclaved at 121 °C for 15 min, acid washed in 20% HCl, and then rinsed with copious amounts of d.i. water.

2.4. Experimental Concept and Design. *2.4.1. Gross Photoreduction Experiment.* O'Driscoll et al. (*15*) and Whalin and Mason (*23*) have suggested that a simple reversible reaction for mercury reduction and oxidation reaction can be written as follows:

$$\mathrm{Hg_r(II)} + \text{photo-reductants} \overset{h\nu}{\rightleftharpoons} \mathrm{DGM} + \text{photo-oxidants} \qquad (1)$$

where $\mathrm{Hg_r(II)}$ in eq 1 refers only to the fraction of divalent mercury species that are available for photoreduction. DGM refers to dissolved gaseous mercury, which is the same as Hg(0).

To follow the kinetics of gross reduction, that is, the reaction

$$\mathrm{Hg_r(II)} + \text{photo-reductants} \xrightarrow{h\nu} \mathrm{DGM} \quad (2)$$

DGM formed in the sample was removed continuously so as to prevent the back-reaction in eq 1 by purging the sample with zero-Hg air (flow rate of 1 L min^{-1}). Hg in the outgoing air was measured with the Tekran 2357B analyzer (Figure 1A).

In a typical experiment, a precleaned and sterile quartz beaker is filled with 200 mL of filtered or unfiltered ocean water, and is capped with the silicone stopper, with Teflon inlet and outlet tubes. The required number of UV-A, or UV-B lamps are then fixed at appropriate locations in the photoreactor. Before starting the UV irradiation, the sample is purged with zero-Hg air for 15−20 min in the dark to remove natural DGM from the sample. Lindberg et al. (*27*) have plotted the DGM remaining in the sample with respect to time and determined the rate constant for DGM removal by purging to be of order 6−7 h^{-1}. We followed this approach to plot the DGM remaining in the sample with respect to time, and determined the rate constant for removal of DGM by purging to be of the order of 20 h^{-1}.

Once DGM readings under dark have dropped to zero, the UV lamp(s) are turned on. Therefore, DGM readings that are measured after the start of UV irradiation are the result of the photoreduction of reducible mercury present in the sample.

Assuming pseudofirst order kinetics, the following equations apply:

$$\frac{\mathrm{d[Hg_r(II)]}}{\mathrm{d}t} = -k_r[\mathrm{Hg_r(II)}] \quad (3)$$

$$\frac{\mathrm{d[DGM]}}{\mathrm{d}t} = k_r[\mathrm{Hg_r(II)}] \quad (4)$$

where k_r is the pseudofirst order rate constant for gross reduction under the experimental conditions.

The sample is irradiated until no further $Hg_r(II)$ is available for reduction, and DGM in the purge gas stream measured by the Tekran Analyzer is consistently below detection limits. All samples were irradiated for at least 17 h, even if the amount of DGM in the purge gas stream remained below detection for many hours. Thus, the forward reaction was driven to completion in this experiment.

Since [DGM] = 0 at time $t = 0$, the total amount of DGM that is removed from the sample via photoreduction is equal to the amount of reducible divalent mercury, $Hg_r(II)$, that was available in the sample. Using this information and eqs 3 and 4 k_r is calculated by fitting the experimental data. Control samples kept in dark showed no DGM production with time.

2.4.2. Net Photoreduction Experiment. Samples for net photoreduction experiments were taken from the same containers that supplied samples for gross photoreduction to ensure that factors like total reducible Hg(II), DOC, etc. were identical.

Assuming that the photoredox reactions are pseudofirst order and reversible, eq 1 can be rewritten as (*15, 23*)

$$\mathrm{Hg_r(II)} \underset{k_o}{\overset{k_1}{\rightleftharpoons}} \mathrm{DGM} \quad (5)$$

where k_o is the rate constant for oxidation of DGM. Equation 5 implies that DGM concentration at any time is the net result of reduction and oxidation reactions. Therefore, in our net photoreduction experiment, we allow both forward and backward reactions to take place by not purging DGM. Since k_r is already known, we expected to calculate k_o from fitting the experimental data.

In a typical net photoreduction experiment, 2.5−3 L of ocean water is purged in dark with zero-Hg air for 45−60 min to remove existing DGM. The DGM-free water is then distributed among eight quartz beakers. Each beaker is filled to the top, with 270−280 mL of sample, with little to no headspace inside the beaker. One beaker is kept in a dark box for control, and the remaining seven beakers are put inside the photoreactor and irradiated (Figure 1B). Thereafter, one beaker at a time is taken out after target irradiation times of 1, 2, 5, 8, 12, 18, and 24 h. A 200 mL subsample is then analyzed for DGM inside a dark box (Figure 1B). Thus, we obtain values of DGM that are produced as a result of net photoreduction inside the quartz beakers over a time period of 24 h (Figure 2B). Control samples, analyzed after 24 h, showed no appreciable change in DGM. F2

3. Results and Discussions

3.1. Kinetic Fitting and Rate Constants. Kinetic curve fitting of experimental data was done using least-squares minimization by a Newton-Gauss algorithm (*28*). For further information see SI Section S3.2.

3.1.1. Gross Photoreduction. We plotted cumulative DGM produced during photoreduction versus time (*15*). A typical example of the curve obtained from experiments and the fitted curve is shown in Figure 2A. Curves for all the other experiments and the corresponding fits are shown in SI Figure S2. The assumption of a pseudofirst order kinetics for gross reduction generally leads to a good fit with experimental results.

The values for k_r are in the range 0.15−0.93 h^{-1}. Individual values of k_r with relation to the radiation intensity are shown in Figure 3. These values are in similar range as those reported for natural freshwater, 0.32−0.65 h^{-1} for UV-B radiation and F3

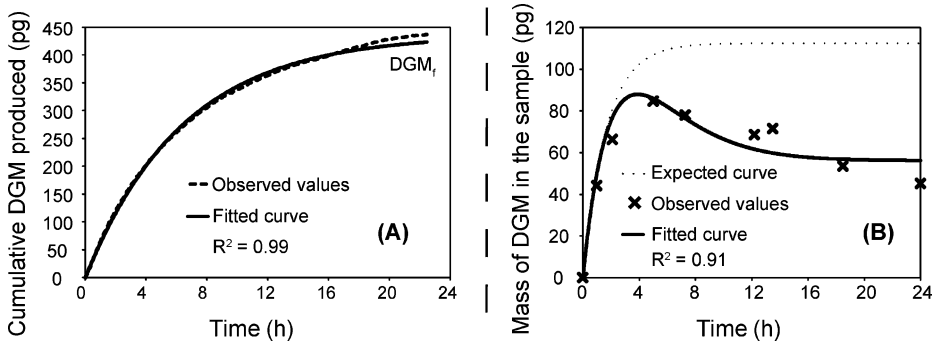

FIGURE 2. Illustration of kinetic curve fitting for (A) gross photoreduction experiment and (B) net photoreduction experiment, when unfiltered ocean water was irradiated with UV-A radiation (39% full sun's intensity, 15.2 W m^{-2}). Note the different legends. The dotted line in (B) is the curve expected from a simple two-species reversible reaction between $Hg_r(II)$ and DGM/ Hg(0), however, observations implied the presence of an intermediate species. The new pathways led to the fitted curve (solid line, obtained using pathway I for this case) which matches the observed values better.

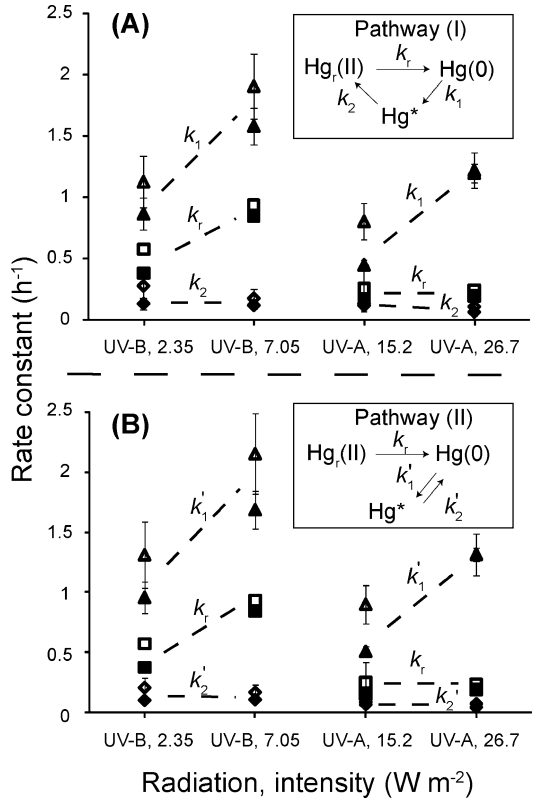

FIGURE 3. Rate constants for reduction of Hg$_r$(II) and (A) oxidation of Hg(0) to Hg* and conversion of Hg* to Hg$_r$(II) for pathway (I); (B) oxidation of Hg(0) to Hg* and conversion of Hg* to Hg(0) for pathway (II); open symbols for filtered samples, and closed symbols for unfiltered samples. Error bars represent one standard deviation of the errors associated with the kinetic fitting.

0.28−0.65 h^{-1} for UV-A radiation (*15*), and are in the lower range of k_r values for spiked near-shore coastal, estuarine, and coastal shelf water, 0.1−9 h^{-1} (*20*).

The pseudofirst order rate constants for gross reduction in filtered samples are equal to or slightly greater than the corresponding rate constants for reduction in unfiltered samples (Figure 3). This could be due to the blocking of radiation or sequestration of DGM from solution by particles. Both possibilities will reduce the apparent reduction efficiency. Overall, the presence of microbes and colloidal matter did not remarkably influence the mercury reduction kinetics. The inference of a negligible influence of biotic reactions is reasonable since the pseudofirst order rate constants for biotic reduction reported in literature (*6, 16*) are of the order of 10^{-4} h^{-1} which is significantly smaller than the pseudofirst order rate constants for abiotic reduction estimated in our work, of order 10^{-1} h^{-1}. Therefore, our results indicate that abiotic reduction dominates biotic reduction of mercury near the surface of the ocean. This dominance likely decreases with the depth of the ocean column due to the decreased light penetration (see SI Section S4 for a further analysis).

UV-B radiation is a more effective driver of reduction reactions in the surface ocean water than UV-A (Figure 3). In a separate experiment (results not shown), we also found that mercury reduction did not take place if a filtered sample was exposed to UV-A intensities lower than 7.6 W m^{-2} (19% of full sun's UV-A intensity as noted in SI Section 2.3.1). Reduction rate constants show an increase with increase in UV-B radiation intensity, but no such increase is observed for UV-A radiation intensity (Figure 3).

3.1.2. Net Photoreduction Experiment to Estimate Pseudofirst Order Rate Constant for Gross Photooxidation. If mercury reduction−oxidation is a simple reversible reaction, that is, if eq 5 describes the reaction pathway, then the DGM present in the sample in the net photoreduction experiment should rise exponentially to a maximum and then stay at this maximum value thereafter (dotted line in Figure 2B). However, we observed that in all the net photoreduction experiments, DGM concentrations reached a maximum, usually within 1−5 h, and then decreased with time to a nonzero value after 24 h of irradiation; an example is shown in Figure 2B, and results from all experiments are shown in SI Figure S3. Therefore, our results indicate that mercury reduction and oxidation in ocean water is not a simple two-species reversible reaction.

Instead, our results imply that oxidation of DGM, as represented by Hg(0), produces a mercury species that is different from the reducible form of Hg(II) present in the sample at the beginning of the experiment. We term this new mercury species Hg* and propose two alternative reaction pathways involving Hg* that can be written as follows.

(i) Pathway (I) (Figure 3A):

$$\mathrm{Hg_r(II)} \xrightarrow{k_r} \mathrm{Hg(0)} \quad (6)$$

$$\mathrm{Hg(0)} \xrightarrow{k_1} \mathrm{Hg^*} \quad (7)$$

$$\mathrm{Hg^*} \xrightarrow{k_2} \mathrm{Hg_r(II)} \quad (8)$$

where k_1 is the rate constant for conversion of Hg(0) to Hg* and k_2 is the rate constant for conversion of Hg* to Hg$_r$(II).

(ii) Pathway (II) (Figure 3B):

$$\mathrm{Hg_r(II)} \xrightarrow{k_r} \mathrm{Hg(0)} \quad (9)$$

$$\mathrm{Hg(0)} \xrightarrow{k'_1} \mathrm{Hg^*} \quad (10)$$

$$\mathrm{Hg^*} \xrightarrow{k'_2} \mathrm{Hg(0)} \quad (11)$$

where k_1' is the rate constant for conversion of Hg(0) to Hg* and k_2' is the rate constant for conversion of Hg* to Hg(0). The corresponding rate laws for the two pathways are shown in SI Section S3.1. It can be hypothesized that Hg* in both the above pathways is an oxidized mercury species, which is forming complexes with chloride (see SI Section S3.3).

Either of the above three-species pathways can account for the observations in the net photoreduction experiments. An example is shown in Figure 2B (solid line); curve fittings for other experiments are shown in SI Figure S3. From Figure 2B, it is also clear that if the experiments are run only for 1 or 2 h, it is not possible to distinguish between the simple reversible pathway and the three-species pathways since concentrations of DGM rise approximately exponentially during this initial phase. This is probably the reason why previous studies conducted for determination of both gross reduction and oxidation (e.g., ref *20*) did not require a three-species pathway to fit their data.

The values of pseudofirst order rate constants obtained after kinetic fitting to either of the two pathways (I) and (II) are summarized in Figure 3; the errors associated with this kinetic fitting, expressed as one standard deviation, are illustrated by the corresponding error bars in the figure. k_1

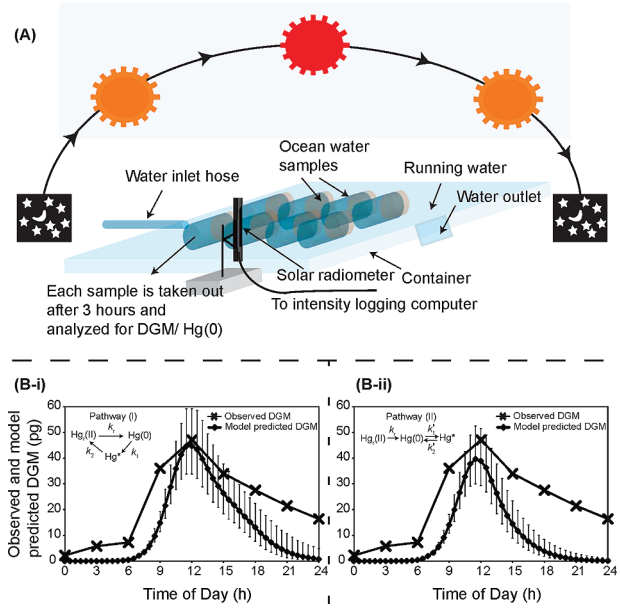

FIGURE 4. (A) Controlled outdoor experiment to monitor the diel variation of DGM mass during the course of 24 h, from midnight to midnight. This information was used to evaluate the pathways shown in B-i and B-ii; (B) Observed and model predicted DGM mass in the samples during the course of the experiment for (i) pathway (I) and (ii) pathway (II). Error bars represent the 95% confidence range of the modeled DGM values.

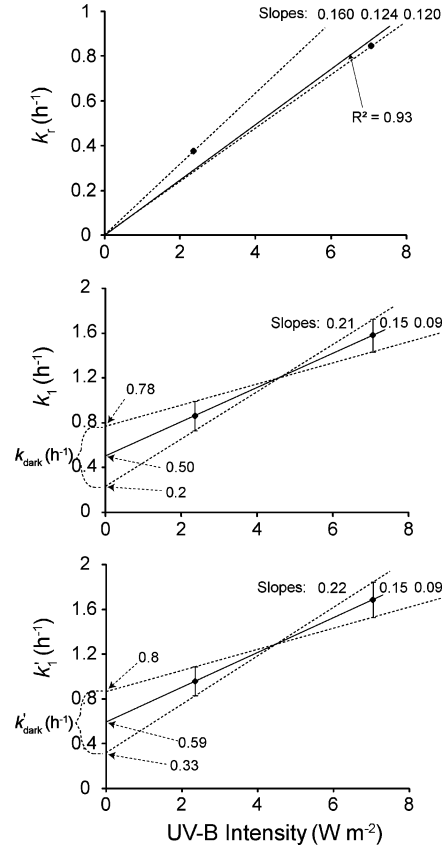

FIGURE 5. Determination of slopes for the pseudofirst order photosensitive rate constants-light intensity linear relationships and determination of the pseudofirst order dark oxidation rate constant, used in the evaluative modeling of Figure 4.

or k_1', the pseudofirst order rate constant for oxidation, for filtered samples is equal to or slightly greater than k_1 or k_1' for unfiltered samples. Therefore, the presence or absence of microbes and colloidal matter did not influence mercury oxidation kinetics appreciably. Furthermore, estimated values for k_1 or k_1' increase with increasing radiation intensity for both UV-B and UV-A radiations. However, the pseudofirst order rate constants k_2 and k_2' are independent of the intensity of radiation and have similar values for both filtered and unfiltered water samples. For all samples and radiation intensities we find that k_1 or $k_1' > k_r > k_2$ or k_2'.

3.2. Evaluation of the Two Alternative Reaction Pathways for Mercury Reduction and Oxidation. To further evaluate the two proposed pathways (I) and (II), we compared the observations made during a 24 h outdoor experiment with the values predicted by models based on either of the two pathways (eqs 6−8 or 9−11), as is described below.

3.2.1. Design of the 24 h Outdoor Experiment. In this experiment, eight quartz beakers filled with unfiltered ocean water were kept outdoors in a constant temperature bath from midnight to midnight (Figure 4A). Solar radiation intensity information (SI Figure S4) was recorded using a Solar radiometer (Ocean Optics USB 4000 with 200 μm fiber optic cable, calibrated for radiometry using DH-2000 UV−vis calibration source). Every 3 h, a beaker was removed and measured for mass of DGM formed.

3.2.3. Model Set-Up and Input Parameters. Computer models were constructed based on the two proposed redox pathways, that is, either eqs 6−8 or eqs 9−11. All input parameters, their values and their corresponding 95% confidence limits (confidence factors, CFs) are listed in SI Table S1. In the model, rate constants are assumed to be a linear function of the incident UV-B radiation (Figure 5 and SI Table S1). Uncertainties in the model are considered by means of a Monte Carlo analysis. The set up of the model input parameters and associated uncertainties are described in the SI Section S5. We made 5000 Monte Carlo simulations to consider the wide range of input value possibilities. The model output predicts the concentrations of DGM at various times of the day along with the associated uncertainties for both the proposed pathways. These predicted DGM concentrations were then compared with the results of the experiment described in Section 3.2.1.

3.2.3. Comparison of Experimental and Model Results. The observed profile of DGM from the 24 h experiment shows a diel pattern (Figure 4B-i and B-ii) in which the amount of DGM in the sample increases after sunrise, reaches a maximum and then decreases gradually to a nonzero value. Similar diel variability has been reported in the natural environment (e.g., refs *11 and 12*).

On the basis of our modeling, we are not able to conclude which of pathways (I) or (II) provides a better description of the observations (Figure 4B-i and B-ii). Sensitivity analysis indicated that the input "dark-oxidation" rate constant is the most important parameter influencing predicted DGM values in the latter half of the curve when they are decreasing, particularly after 6:00 pm (>80% contribution to variance in the model predicted values). It must be noted that the input dark oxidation rate constant used by us may represent an upper limit of possible values (see SI Section S5.1); a lower input value will increase the model predicted values and improve the agreement with observations.

3.3. Future Outlook. The work reported here contributes to the reduction of uncertainties in the rates of reduction and oxidation reactions of mercury in surface ocean water and the corresponding pathways of these reactions, as has been recently called for (*25*). Pseudofirst order rate constants have been determined for filtered and unfiltered surface ocean water under UV-A and UV-B radiation. Our results, extrapolated using diffuse attenuation coefficients, suggest that for the top 10 m of ocean waters, the day and depth-averaged rate constant for abiotic reduction is likely at least

1 order of magnitude greater that the reported rate constants for biotic reduction (see SI Section S4). We also report new information that suggests a three-species pathway for the reduction/ oxidation reaction. Future experiments should focus on further elucidating and differentiating the two proposed three-species pathways and on characterization of Hg*. Furthermore, it is important to characterize the reducible fraction of total mercury in water. It will also be useful to further constrain the rate constant for dark oxidation, and to obtain the thermodynamic temperature component of the pseudofirst order rate constants. Finally, it will be worthwhile to conduct experiments similar to ours on ocean water samples from different locations to test our hypothesized three-species pathways.

Acknowledgments

Funding for this work was provided by the Swiss Federal Office for the Environment (Bundesamt für Umwelt, BAFU) and grants to N.O. from the National Science and Engineering Council of Canada (NSERC), the Canada Research Chairs Program (CRC), and the Canada Foundation for Innovation (CFI).

Supporting Information Available

Eleven pages of text, Figures S1−S4 and Table S1. This material is available free of charge via the Internet at http://pubs.acs.org.

Literature Cited

(1) Mason, R. P., Sheu, G.-R. Role of ocean in the global mercury cycle. Global Biogeochem. Cyc. 2002, *16*, doi: 10.1029/2001GB001440.

(2) Amyot, M.; Gill, G. A.; Morel, F. M. M. Production and loss of dissolved gaseous mercury in coastal seawater. *Environ. Sci. Technol.* **1997**, *31*, 3606–3611.

(3) Amyot, M.; Mierle, G.; Lean, D. R. S.; McQueen, D. J. Sunlight-induced formation of dissolved gaseous mercury in lake waters. *Environ. Sci. Technol.* **1994**, *28*, 2366–2371.

(4) Zhang, H.; Lindberg, S. E. Sunlight and iron(III)-induced photochemical production of dissolved gaseous mercury in freshwater. *Environ. Sci. Technol.* **2001**, *35*, 928–935.

(5) Amyot, M.; Southworth, G.; Lindberg, S. E.; Hintelmann, H.; Lalonde, J. D.; Ogrinc, N.; Poulain, A. J.; Sandilands, K. A. Formation and evasion of dissolved gaseous mercury in large enclosures amended with $^{200}HgCl_2$. *Atmos. Environ.* **2004**, *38*, 4729–4289.

(6) Mason, R. P.; Morel, F. M. M.; Hemond, H. F. The role of microorganisms in elemental mercury formation in natural waters. *Water Air Soil Poll.* **1995**, *80*, 775–787.

(7) Siciliano, S. D.; O'Driscoll, N. J.; Lean, D. R. S. Microbial reduction and oxidation of mercury in freshwater lakes. *Environ. Sci. Technol.* **2002**, *36*, 3064–3068.

(8) Voughan, P. P.; Blough, N. V. Photochemical formation of hydroxyl radical by constituents of natural waters. *Environ. Sci. Technol.* **1998**, *32*, 2947–2953.

(9) Lalonde, J. D.; Amyot, M.; Kraepiel, A. M. L.; Morel, F. M. M. *Photooxidation of Hg(0) in artificial and natural waters. Environ. Sci. Technol.* **2001**, *35*, 1367–1372.

(10) Lalonde, J. D.; Amyot, M.; Orvoine, J.; Morel, F. M. M.; Auclair, J.-C.; Ariya, P. A. Photoinduced oxidation of Hg^0(aq) in the waters from the St. Lawrence Estuary. *Environ. Sci. Technol.* **2004**, *38*, 508–514.

(11) Lanzillotta, E.; Ferrara, R. Daily trend of dissolved gaseous mercury concentration in coastal seawater of the Mediterranean basin. *Chemosphere* **2001**, *45*, 935–940.

(12) O'Driscoll, N. J.; Siciliano, S. D.; Lean, D. R. S. Continuous analysis of dissolved gaseous mercury in freshwater lakes. *Sci. Total Environ.* **2003**, *304*, 285–294.

(13) Garcia, E.; Poulain, A. J.; Amyot, M.; Ariya, P. Diel variations in photoinduced oxidation of Hg^0 in freshwater. *Chemosphere* **2005**, *59*, 977–981.

(14) Xiao, Z. F.; Strömberg, D.; Lindqvist, O. Influence of humic substances on photolysis of divalent mercury in aqueous solution. *Water Air Soil Poll.* **1995**, *80*, 789–798.

(15) O'Driscoll, N. J.; Siciliano, S. D.; Lean, D. R. S.; Amyot, M. Gross photoreduction kinetics of mercury in temperate freshwater lakes and rivers: application to a general model of DGM dynamics. *Environ. Sci. Technol.* **2006**, *40*, 837–843.

(16) Strode, S. A., Jaeglé, L., Selin, N. E., Jacob, D. J., Park, R. J., Yantosca, R. M., Mason, R. P., Slemr, F. Air-sea exchange in the global mercury cycle. Global Biogeochem. Cy. 2007, *21*, doi: 10.1029/2006GB002766.

(17) Allard, B.; Arsenie, I. Abiotic reduction of mercury by humic substances in aquatic system - an important process for the mercury cycle. *Water Air Soil Poll.* **1991**, *56*, 457–464.

(18) Gårdfeldt, K.; Jonsson, M. Is bimolecular reduction of Hg(II) complexes possible in aqueous systems of environmental importance. *J. Phys. Chem. A* **2003**, *107*, 4478–4482.

(19) Spokes, L. J.; Liss, P. S. Photochemically induced redox reactions in seawater, I. Cations. *Mar. Chem.* **1995**, *49*, 201–213.

(20) Whalin, L.; Kim, E.-H.; Mason, R. Factors influencing the oxidation, reduction, methylation and demethylation of mercury species in coastal waters. *Mar. Chem.* **2007**, *107*, 278–294.

(21) Krabbenhoft, D. P.; Hurler, J. P.; Olson, M. L.; Cleckner, L. B. Diel variability of mercury phase and species distributions in the Florida Everglades. *Biogeochemistry* **1998**, *40*, 311–325.

(22) Mason, R. P.; Lawson, N. M.; Sheu, G.-R. Mercury in the Atlantic Ocean: factors controlling air-sea exchange of mercury and its distribution in the upper waters. *Deep-Sea Res. II* **2001**, *48*, 2829–2853.

(23) Whalin, L. M.; Mason, R. P. A new method for the investigation of mercury redox chemistry in natural waters utilizing deflatable Teflon® bags and additions of isotopically labeled mercury. *Anal. Chim. Acta* **2006**, *558*, 211–221.

(24) Selin, N. E., Jacob, D. J., Park, R. J., Yantosca, R. M., Strode, S., Jaeglé, L., Jaffe, D. Chemical cycling and deposition of atmospheric mercury: global constraints from observations. J. Geophys. Res. 2007, *112*, doi:10.1029/2006JD007450.

(25) Pirrone, N., Hedgecock, I. M., Sprovieri, F. New directions: atmospheric mercury, easy to spot and hard to pin down: impasse? Atmos. Environ. 2008, doi: 10.1016/j.atmosenv.2008.09.004.

(26) Mazur, P. Physical factors implicated in the death of microorganisms at subzero temperatures. *Ann. N.Y. Acad. Sci.* **1960**, *85*, 610–629.

(27) Lindberg, S. E.; Vette, A. F.; Miles, C.; Schaedlich, F. Mercury speciation in natural waters: measurement of dissolved gaseous mercury with a field analyzer. *Biogeochem.* **2000**, *48*, 237–259.

(28) Maeder, M., Neuhold, Y.-M. *Practical data analysis in chemistry*; Elsevier Science Publishers: Amsterdam, Netherlands, 2007.

ES9012728